Int J Thermophys (2009) 30:2021–2035
DOI 10.1007/s10765-009-0680-5

Inverse Identification of Thermal Properties of Fibrous Insulation from Transient Temperature Measurements

Shu-yuan Zhao · Bo-ming Zhang · Shan-yi Du · Xiao-dong He

Received: 9 April 2009 / Accepted: 5 November 2009 / Published online: 25 November 2009

Abstract In this article, an experimental setup was developed to measure the transient temperature response in fibrous insulation. The radiative properties were modified to take anisotropic scattering in fibrous insulation into account. A model of combined radiation and conduction heat transfer through fibrous insulation was generated based on the two-flux approximation. Using the measured transient temperature response, the Levenberg–Marquardt method was utilized to identify the equivalent radiative properties and thermal conductivities of fibrous insulation. The identified thermal properties were validated by transient and steady state experimental results of fibrous insulation. Satisfactory agreement was obtained.

Keywords Insulation · Inverse · Radiative properties · Thermal conductivity · Transient temperature measurements

1 Introduction

Heat transfer through highly porous fibrous materials is a problem of considerable interest because of the widespread use of fiber composites in many areas such as the development of thermal protection systems for reusable launch vehicles and other commercial thermal insulation systems.

Heat transfer in low-density fibrous media may be by any of four mechanisms, namely, convection, fiber conduction, air conduction, and radiation. It has been shown that convective heat transfer is absent or minimal in fibrous insulation [1]. Conduction by the fibers is minimal because of the low density of the media, at most, a few

S. Zhao (✉) · B. Zhang · S. Du · X. He
Center for Composite Materials and Structure, Harbin Institute of Technology, Harbin 150080, China
e-mail: angel.zsy@126.com

percent of the total heat flow. The dominant mechanisms of heat flow are conduction by the air and radiation. Previous studies about heat transfer through fibrous media have shown that radiative heat transfer accounts for 40 % to 50 % of the total heat transfer in light-weight fibrous insulation at moderate temperatures [2]. The energy transport process in fibrous insulation under aerodynamic heating conditions is complicated with increasing temperature, which makes the analysis and design of insulation quite difficult. In order to better understand energy transport in fibrous media, extensive research has been carried out over recent decades. The researchers developed an effective thermal conductivity model based on superposition of gas, solid, and apparent radiation thermal conductivities, based on the optically thick assumption, and compared the results with measured effective thermal conductivities of samples subjected to certain temperature difference across the insulation thickness [3,4]. Tong et al. [5–7] used the two-flux model assuming linearized anisotropic scattering to model radiation heat transfer through fibrous insulation, and the predicted fluxes that combined radiant and conduction heat transfer were compared with measured data up to 450 K and at one atmosphere. Marschall et al. [8] used temperature transients computed with a radiation–conduction model as input to a parameter estimation routine to extract dynamic effective conductivities and compared these to static values. Daryabeigi [9] modeled heat transfer in alumina fibrous insulation to predict effective thermal conductivities. A genetic-algorithm-based parameter estimation technique was utilized to determine the relevant radiative properties of fibrous insulation. Walter et al. [10] used a first-principle approach to analyze combined conductive/radiative heat transfer in high porosity silica insulation materials (LI900) used by the Space Shuttle. Macroscopic average radiative properties such as the extinction coefficient, scattering albedo, and phase function were generated by solving the radiative transfer equation for fibrous insulation using the measured value of the refractive index (n, k). The calculated transient temperatures were compared with experimental data.

In this study, an experimental setup is developed to measure the transient temperature response in fibrous insulation. A model of combined radiation and conduction heat transfer through fibrous insulation is generated based on the two-flux approximation. The measured radiative properties are modified to take anisotropic scattering in fibrous insulation into account. Using the measured transient temperature response, an inverse technique is utilized to identify the thermal properties of fibrous insulation. Then the identified thermal properties are validated.

2 Experiment

A transient thermal test setup was developed to characterize the transient thermal behavior of the insulation. A schematic of the transient thermal test setup is shown in Fig. 1. In order to provide rapid transient heating and cooling required in a typical re-entry profile, a quartz lamp radiant heating array with low thermal mass is used to serve as a radiant heat source. The heating array consists of 21 quartz lamps (diameter of 12 mm, length of 760 mm, power of 3 kW). The array is powered by a phase angle-fired, silicon control rectifier (SCR) power controller

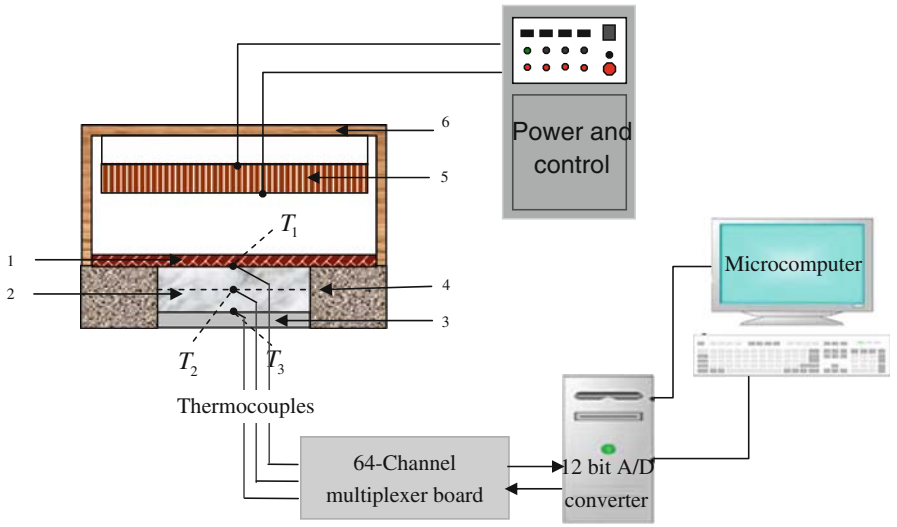

1. Septum plate; 2. Test specimen assembly; 3. Aluminum plate; 4. Guarded insulation; 5. Quartz lamp array; 6. Water-cooled reflector

Fig. 1 Schematic of transient thermal testing apparatus

and a 380 VAC, three-phase transformer. It can provide a time variant surface temperature for the measurement of the temperature distribution in fibrous insulation under transient heating conditions. A water-cooled reflector around the heating array helps to achieve the cooling rates necessary for the latter stages of the re-entry profile. The fibrous insulation to be tested is located between a septum plate and an aluminum plate. In addition to its function in simulating the backside boundary condition, the aluminum plate is used as a platform for the test sample. Guarded insulation boards are placed around the test specimen to minimize heat loss and provide in the course of testing a temperature distribution in the specimen close to one-dimensional. Twelve Type-K thermocouples are installed to monitor the changes of temperature distribution during heating and cooling. The sensor locations of the septum plate and the aluminum plate are specified in Figs. 2 and 3, respectively. One thermocouple in the central region of the septum plate is used for feedback control. $T_1(t)$, $T_2(t)$, and $T_3(t)$ which are shown in Fig. 1 correspond to the time-varying temperatures at through-thickness locations of $x = 0\,\text{mm}$, $x = 20\,\text{mm}$, and $x = 40\,\text{mm}$, respectively. Signals from the thermocouples are transmitted to a computerized data acquisition system for recording measurement data via a multi-channel temperature measurement device in conjunction with personal-programmed data acquisition software. The measured transient temperatures can be used for identification of thermal properties and validation of numerical models.

The insulation sample studied in this investigation is aluminosilicate fibrous insulation with a nominal density of $128\,\text{kg}\cdot\text{m}^{-3}$. The test specimen is a slab configuration of 200 mm square. The experiment is conducted in air at atmospheric pressure. Two heating modes are set for the current investigation. The first heating mode is to set

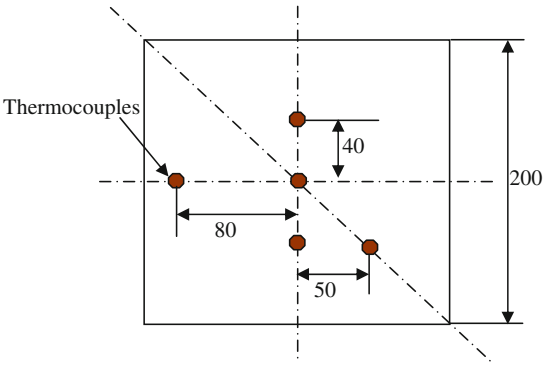

Fig. 2 Sensor locations at hot side (mm)

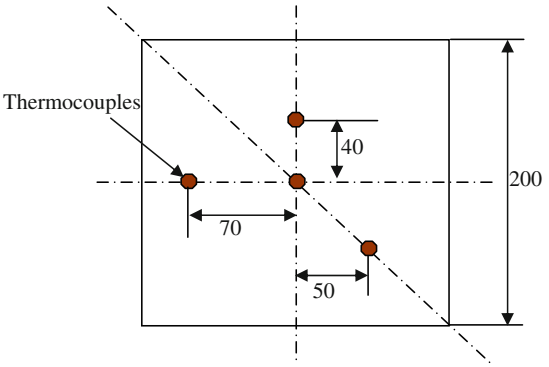

Fig. 3 Sensor locations at cold side (mm)

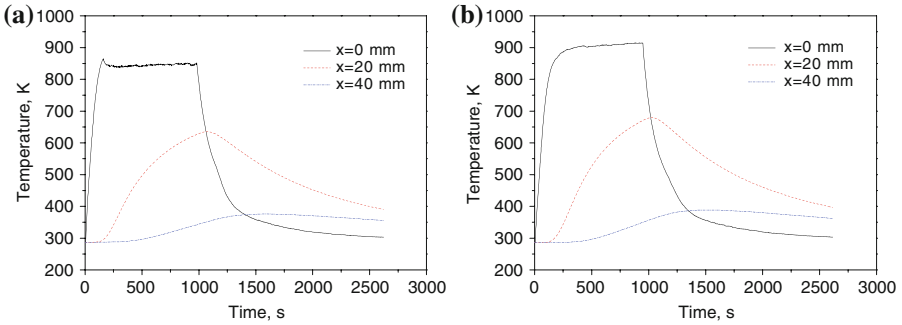

Fig. 4 Measured transient temperature response of fibrous insulation sample: **(a)** heating mode 1 and **(b)** heating mode 2

the hot-side-temperature rise from 290 K to 850 K in 140 s and hold at 850 K for 840 s, and then the sample is gradually cooled. The second heating mode is to set the hot-side-temperature rise from 290 K to 910 K in 350 s and hold at 910 K for 600 s, and then the sample is gradually cooled. The measured front and back surface temperatures and internal temperature responses of fibrous insulation at a depth of 20 mm using the experimental setup are shown in Fig. 4. In order to check the temperature

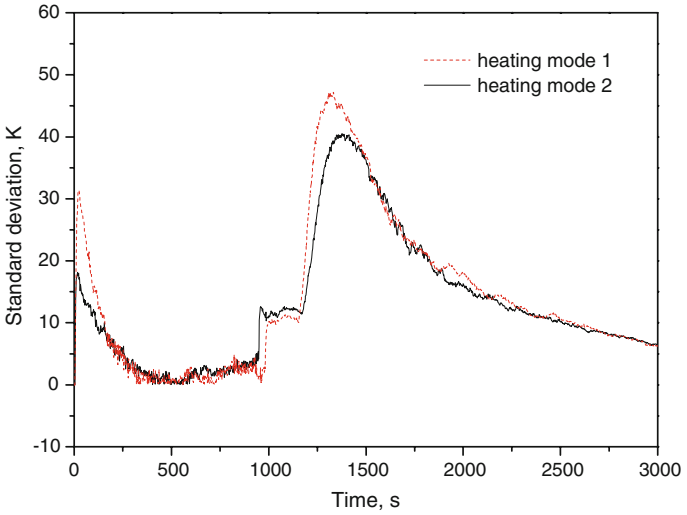

Fig. 5 Standard deviation of the measured hot-side temperatures for test on fibrous insulation sample

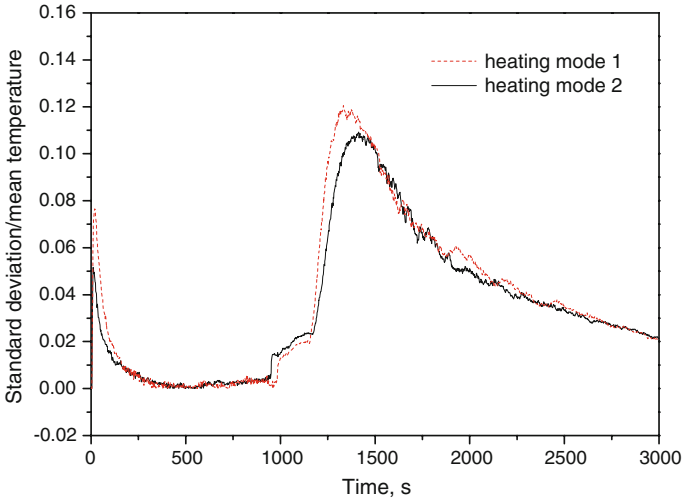

Fig. 6 Ratio of standard deviation to mean temperature for the hot-side-temperature measurement

uniformity of the test specimen, the statistical variations of the hot-side-temperature measurements were studied. The standard deviation and the ratio of standard deviation to the mean temperature in temperature measurements are shown in Figs. 5 and 6, respectively. The estimated maximum uncertainty in the temperature measurements is about 47.2 K. The temperature distribution over the surface of the test specimen is uniform to within ± 12 %.

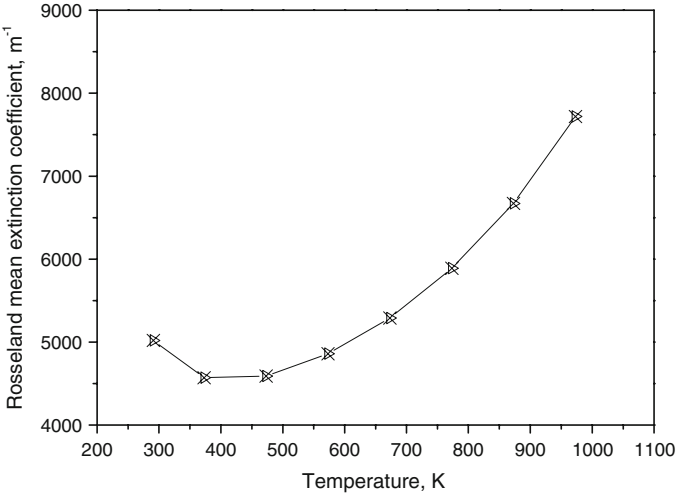

Fig. 7 Variation of Rosseland mean extinction coefficient with temperature

3 Analysis

3.1 Radiative Properties

A knowledge of spectral and temperature dependencies of the extinction coefficient and the albedo of scattering is required to investigate radiative heat transfer within fibrous insulation. The spectral transmittance of the fibrous insulation in the wavelength range of 2.5 μm to 25 μm was measured over the temperature range of 291 K to 973 K using a Fourier transform infrared spectrometer [11]. The spectral extinction coefficients were calculated using the measured transmittance data by means of Beer's law. The Rosseland mean extinction coefficients, K_{R}, were obtained according to the following equation [12]:

$$\frac{1}{K_{\mathrm{R}}} = \int_0^\infty \frac{1}{\beta_\lambda} \frac{\partial e_{\mathrm{b}\lambda}}{\partial e_{\mathrm{b}}} \mathrm{d}\lambda \approx \int_a^b \frac{1}{\beta_\lambda} \frac{\partial e_{\mathrm{b}\lambda}}{\partial e_{\mathrm{b}}} \mathrm{d}\lambda \tag{1}$$

with $a = 2.5\,\mu\mathrm{m}$ and $b = 25\,\mu\mathrm{m}$ in this study. λ is the wavelength, e_{b} is the blackbody emissive power, $e_{\mathrm{b}\lambda}$ is the spectral blackbody emissive power, and β_λ is the spectral extinction coefficient. The obtained Rosseland mean extinction coefficient K_{R} is shown in Fig. 7 [11].

To take into account anisotropic scattering by insulation, a weighted spectral scattering coefficient $\sigma^*_{\mathrm{s}\lambda}$ is defined as [13]:

$$\sigma^*_{\mathrm{s}\lambda} = \sigma_{\mathrm{s}\lambda}(1 - g_\lambda) \tag{2}$$

where g_λ is the anisotropy factor.

The weighted spectral extinction coefficient β_λ^* substitutes for the real spectral extinction coefficient β_λ.

$$\beta_\lambda^* = \sigma_{a\lambda} + \sigma_{s\lambda}^* \tag{3}$$

where $\sigma_{a\lambda}$ is the spectral absorption coefficient.

The weighted spectral albedo of scattering, which is defined as the ratio of the weighted scattering coefficient to the weighted extinction coefficient, is given by:

$$\omega_\lambda^* = \frac{\sigma_{s\lambda}^*}{\beta_\lambda^*} = \frac{\sigma_{s\lambda}(1-g_\lambda)}{\beta_\lambda - \sigma_{s\lambda} g_\lambda} \tag{4}$$

From Eqs. 2–4, β_λ^* can be obtained as

$$\beta_\lambda^* = \frac{1-g_\lambda}{1-g_\lambda+\omega_\lambda^* g_\lambda}\beta_\lambda \tag{5}$$

Equation 5 is substituted into Eq. 1. The weighted spectral scattering coefficient is averaged over the spectrum weighted by the emissive power. Then the following equations can be obtained based on the first mean value theorem for integrals [14]:

$$\frac{1}{K_R^*} = \frac{(1-g_\xi+\omega_\xi^* g_\xi)}{(1-g_\xi)} \int_a^b \frac{1}{\beta_\lambda}\frac{\partial e_{b\lambda}}{\partial e_b} d\lambda \quad \xi \in [a,b] \tag{6}$$

$$\frac{1}{\sigma_s^*} = \frac{1}{\omega_\eta^*} \int_a^b \frac{(1-g_\lambda+\omega_\lambda^* g_\lambda)}{(1-g_\lambda)} \frac{1}{\beta_\lambda}\frac{\partial e_{b\lambda}}{\partial e_b} d\lambda \quad \eta \in [a,b] \tag{7}$$

where σ_s^* is the weighted scattering coefficient.

Therefore, the equivalent Rosseland mean extinction coefficient K_R^* and equivalent albedo of scattering ω^* are obtained as

$$K_R^* = \frac{(1-g_\xi)}{(1-g_\xi+\omega_\xi^* g_\xi)} K_R = f_\xi K_R \tag{8}$$

$$\omega^* = \frac{\sigma_s^*}{K_R^*} = \omega_\eta^* \tag{9}$$

where f_ξ is a modified factor of the extinction coefficient; it represents the ratio of the extinction coefficient with and without taking into account anisotropic scattering.

For more details about the modification of radiative properties refer to [15].

3.2 Conservative Equations

Neglecting the effect of natural convective heat transfer, the conservation of energy for one-dimensional heat transfer through the insulation by conduction and radiation can be written as [16]

$$\rho c \frac{\partial T(x,t)}{\partial t} = \frac{\partial}{\partial x}\left(k_c \frac{\partial T(x,t)}{\partial x}\right) - \frac{\partial q_r''(x,t)}{\partial x} \tag{10}$$

subject to the following initial and boundary conditions,

$$T(x,0) = T_0 \tag{11}$$
$$T(0,t) = T_1(t) \tag{12a}$$
$$T(L,t) = T_3(t) \tag{12b}$$

where T is the temperature, ρ, c, and k_c are, respectively, the density, specific heat, and conductive thermal conductivity of a fibrous insulation sample. q_r'' is the radiant heat flux, t is the time, and x is the spatial coordinate through the insulation thickness. The gradient of the radiant heat flux is given by

$$\frac{\partial q_r''(x,t)}{\partial x} = K_R^*(1-\omega^*)(4\sigma T^4(x,t) - G(x,t)) \tag{13}$$

where σ is the Stefan–Boltzmann constant, $G(x,t)$ is the incident radiation, K_R^* is the weighted Rosseland mean extinction coefficient, and ω^* is the equivalent albedo of scattering. The Milne–Eddington approximation is used to model the radiation heat transfer through fibrous insulation. The radiant heat flux is related to the incident radiation, $G(x,t)$, according to Ozisik [17]

$$q_r''(x,t) = -\frac{1}{3K_R^*}\frac{\partial G(x,t)}{\partial x} \tag{14}$$

The second-order differential equation governing the incident radiation is solved subject to the following boundary conditions:

$$q_r''(0,t) = \frac{\varepsilon_1}{2(2-\varepsilon_1)}[4\sigma T_1^4(t) - G(0,t)] \tag{15a}$$
$$q_r''(L,t) = \frac{\varepsilon_2}{2(2-\varepsilon_2)}[4\sigma T_3^4(t) - G(L,t)] \tag{15b}$$

where ε_1 and ε_2 are the emittances of the upper and lower boundary surfaces, respectively, and $\varepsilon_1 = 0.8$ and $\varepsilon_2 = 0.3$ are used for the current analysis.

4 Parameter Estimation

The modified factor of extinction coefficient f_ξ, the equivalent albedo of scattering ω^*, and the thermal conductivity due to gas and solid conduction k_c are unknown, while data for the variation of temperature with time at different locations can be measured. These temperature data can be used to determine thermal properties by an inverse technique. In this study, the Levenberg–Marquardt iteration method is used to obtain the thermal properties by direct least-squares minimization of the sum of the squared temperature differences between the measured and calculated temperatures. The code

estimates linear f_ξ and k_c variations with temperature by providing the values at two different temperatures.

Then the inverse problem consists of utilizing the measured data $T_{e,i}$to determine the five elements of the unknown vector X defined as

$$\psi(X) = \sum_{i=1}^{N} (T_{e,i} - T_{c,i})^2 = R^T R \tag{16}$$

All of the arguments of X will be referred to as parameters. To minimize $\psi(X)$, the above equation is differentiated with respect to each of the unknown parameters $X \equiv \{x_1, x_2, x_3, x_4, x_5\} = \{f_{\xi 1}, f_{\xi 2}, \omega^*, k_{c1}, k_{c2}\}$ to yield:

$$\frac{\partial \psi(X)}{\partial X} = \frac{\partial (R^T R)}{\partial X} = 0 \tag{17}$$

In this equation, the vector R is expanded in a Taylor series, and only the first-order terms are retained. To improve convergence of the solution of the resulting system of equations, a damping parameter λ is added to yield the Levenberg–Marquardt algorithm [18].

$$(J^T J + I\lambda)\Delta X = J^T R \tag{18}$$

where J is the Jacobian matrix. To obtain the Jacobian matrix, each variable has to be perturbed individually followed by a numerical simulation for each perturbed variable to calculate the value of the objective function. The elements of the Jacobian matrix, $J_{i,j}$, can be calculated by the following finite difference formula:

$$J_{i,j} = \frac{\partial T_{c,i}}{\partial x_j} = \frac{T_{c,i}(x_1, x_2, \ldots, x_j + \Delta x_j, \ldots) - T_{c,i}(x_1, x_2, \ldots, x_j, \ldots)}{\Delta x_j} \qquad i = 1, \ldots, N;\ j = 1, 2, 3, 4, 5 \tag{19}$$

The iterative procedure starts with an initial guess for the vector of unknowns X^0. The iterative procedure at iteration level k, is defined by

$$X^{k+1} = X^k + [(J^k)^T J^k + I\lambda^k]^{-1} (J^k)^T R^k \tag{20}$$

The convergence criterion is

$$\max_{1 \le j \le 5} \left| \frac{x_j^{k+1} - x_j^k}{x_j^k} \right| < \varepsilon \tag{21}$$

$\varepsilon = 10^{-5}$ is used in this study.

95 % confidence intervals of the estimated results are assessed using the standard deviation of x_n [19].

5 Results and Discussion

The experimentally measured specific heat and Rosseland mean extinction coefficient of fibrous insulation from a previous study [12] are substituted in the numerical heat transfer model of the test specimen. The parameter estimation routine repeatedly solves the radiation–conduction model, with iteratively adjusted values of thermal properties, until the best possible agreement is achieved between the measured and computed temperature histories. The solution method involves solving the direct conduction problem with the finite difference method, computing the sensitivity coefficients for each parameter, and calculating the parameters by iteration. The identified thermal properties for the considered two heating modes by the inverse method are shown in Table 1. The obtained thermal properties are used to calculate the transient temperature responses of the insulation sample. The temperature differences between the calculated and the experimental responses at a through-thickness location of $x = 20\,\text{mm}$ are shown in Fig. 8. Clearly, the variation of the temperature difference depends on the period. As for heating mode 1, the largest difference is observed at $t = 984\,\text{s}$, which is about 4.27 K. And at $t = 1130\,\text{s}$, there is the minimum difference, which equals $-3.52\,\text{K}$. However, temperature differences for heating mode 2 vary between $-4.45\,\text{K}$ and $+5.39\,\text{K}$, and the minimum and maximum differences occur at $t = 1109\,\text{s}$ and $t = 178\,\text{s}$, respectively. It is noticed that the minimum temperature differences are observed immediately after the heater was turned off. The small temperature differences for the considered two heating modes indicate small errors in the result of the inverse conduction analysis.

To validate the identified thermal conductivity, the identified results are compared with existing thermal-conductivity models. Several theories have been developed to describe the combined thermal conductivity due to solid and gas conductions. For fibrous composites, the simplest alternatives would be with the materials arranged in either parallel or series with respect to heat flow, which gives the upper or lower bound of the effective thermal conductivity [20]. For the parallel conduction model,

$$k_c = f k_s + (1 - f) k_g, \tag{22}$$

and for the series conduction model,

$$k_c = \frac{k_s k_g}{f k_g + (1 - f) k_s}, \tag{23}$$

where k_g is the gas thermal conductivity and k_s is the solid thermal conductivity.

A combined parallel–series thermal network model for combining gas and solid conductions in fibrous insulation is given by [21]:

$$k_c = \gamma [P_1 k_g + (1 - P_1) k_s] + (1 - \gamma) \frac{k_g k_s}{[P_2 k_f + (1 - P_2) k_g]} \tag{24}$$

where γ is the fraction of the fibers oriented parallel to the heat flux, and P_1 and P_2 are the porosity parameters. The total porosity of the material is $P = \gamma P_1 + (1 - \gamma) P_2$.

Table 1 Estimated thermal properties of fibrous insulation

	f_ξ		ω^*	$k_c(\mathrm{W \cdot m^{-1} \cdot K^{-1}})$	
Heating mode 1	300 K	800 K	0.99900 ± 0.00001	300 K	800 K
	0.96303 ± 0.01625	0.36388 ± 0.00246		0.01745 ± 0.00012	0.03615 ± 0.00021
Heating mode 2	300 K	900 K	0.99899 ± 0.00004	300 K	900 K
	0.74847 ± 0.09047	0.30819 ± 0.01992		0.01659 ± 0.00092	0.04040 ± 0.00071

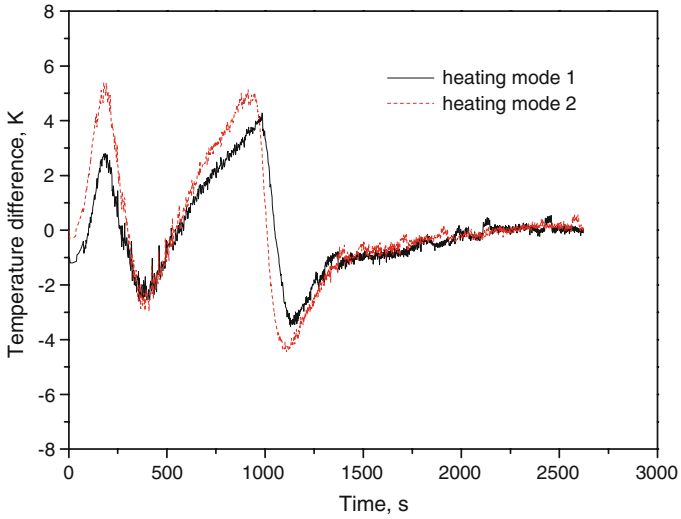

Fig. 8 Difference between the predicted and measured temperatures

For fibers randomly placed and oriented in space, $\gamma = \frac{1}{3}$ and $P_1 = P_2$ were utilized to qualitatively evaluate the fiber conductivity effect according to Dombrovsky [22].

For solid conduction in fibrous insulation, the empirical model can be defined as

$$k_s = f^m k_s^* \tag{25}$$

where f is the solid fraction ratio and k_s^* is the variation of the thermal conductivity of the fiber parent material with temperature. The above equation is based on the model proposed by Verschoor et al. [3]. Hager and Steere [4] used $m = 3$ to model the solid conduction in fibrous insulation and stated that it was an upper-limiting value when contact with the fibers was less than perfect. $m = 2$ was utilized for modeling solid conduction in fibrous insulation spacers in high-temperature multilayer insulations [23]. For alumina fibrous insulation, $m = 1.4$ was determined using a parameter estimation technique in [24]. In the present investigation, $m = 2$ is used. $f = 0.0494$ and $k_s^* = 0.24623 + 0.00149T$ $\mathrm{W \cdot m^{-1} \cdot K^{-1}}$ [25] are used to calculate the solid thermal conductivity.

Comparisons of the estimated thermal conductivities with the existing models are shown in Fig. 9. From this figure, it can be seen that the estimated results exist between the parallel and series results, and they are closer to the results calculated using the combined parallel-series model. It can be stated that $\gamma = \frac{1}{3}$ is applicable to describe the thermal conductivity of fibers randomly placed and oriented in space. For the present fibrous insulation sample, the fibers are stratified randomly, in more or less parallel planes between the medium boundaries from the SEM micrograph [11]. Therefore, the part of the fibers oriented in series to the heat flux for the present sample is larger than that for the fibers randomly placed and oriented in space. It is expected that γ for the present sample should be smaller than 1/3. In order to gain further insight into the actual fraction of the fibers oriented parallel to the heat flux, γ for the current

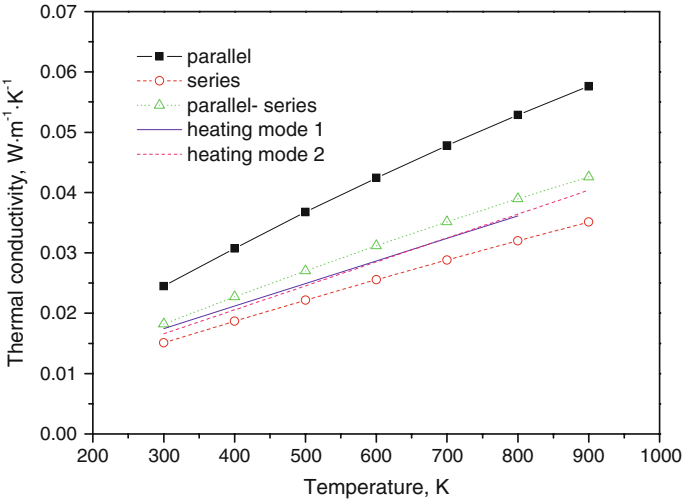

Fig. 9 Comparison of estimated thermal conductivity with existing models

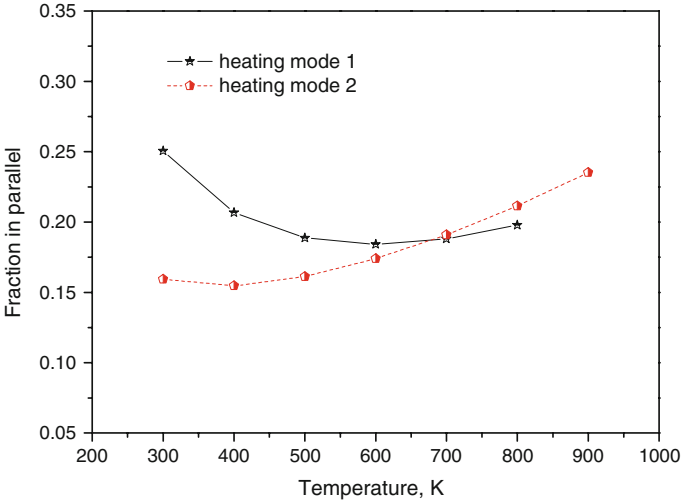

Fig. 10 Variation of fraction of heat transfer in parallel mode with temperature

sample is calculated. Variation of the calculated fraction of heat transfer in the parallel mode with temperature is shown in Fig. 10. It demonstrates that γ varies between 0.16 and 0.25 for the investigated temperature range. Therefore, the estimated thermal conductivity is reliable.

To further validate the estimated thermal properties, the estimated results are used to calculate the effective thermal conductivity, which is then compared with the measured result. The effective thermal conductivity of fibrous insulation was measured based on the YB/T 4130-2005 in Luoyang Institute of Refractories Research (LIRR) [26]. Comparison of experimental and calculated results of the effective thermal con-

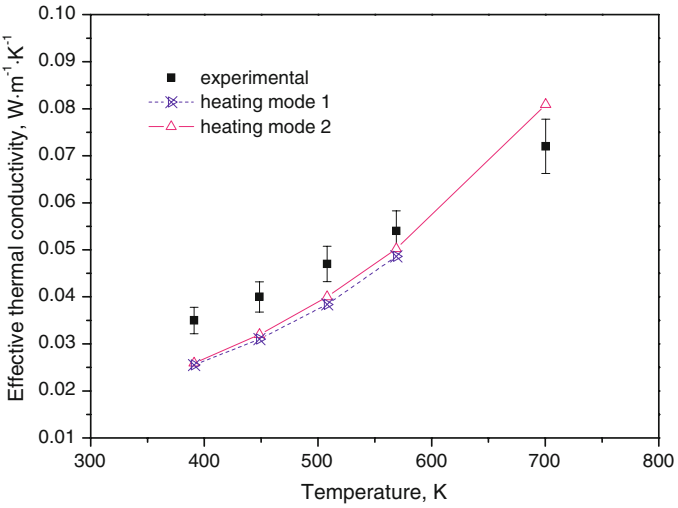

Fig. 11 Comparison of calculated and experimental results of effective thermal conductivity

ductivity using the estimated thermal properties is shown in Fig. 11. As can be seen from this figure, most of the predicted effective thermal conductivities using the estimated thermal properties are under-predicted when compared to the measured data. Although the experiments were designed to set up a one-dimensional transient temperature response, the existence of multi-dimensional heat transport is unavoidable. This phenomenon will generally slow the rate of measured internal temperature rises, which apparently decreases the "dynamic" effective thermal conductivity of fibrous insulation. Therefore, the predicted effective thermal conductivities are smaller than the measured data. The largest deviation between the predicted and measured effective thermal conductivities occurs at low temperature, which is larger than 20 %. At high temperature, the deviation is around 10 %. The average absolute deviation is 17.6 %. Given the complexity of thermal radiation in fibrous insulation and the uncertainty in transient thermal tests, the agreement between theory and experiment is considered reasonable.

6 Conclusions

In this study, an experimental setup was developed to measure the transient temperature response in fibrous insulation. The measured radiative properties were modified to take anisotropic scattering in fibrous insulation into account. A model of combined radiation and conduction heat transfer through fibrous insulation was generated based on the two-flux approximation. Using the measured transient temperature response, an inverse technique was utilized to identify the thermal properties of fibrous insulation. The identified thermal properties were used to calculate the transient temperature response of the fibrous specimen. It was found that the temperature differences between the calculated and the experimental responses for the considered heating modes were

within ±5.4 K, which indicated small errors in the result of the inverse conduction analysis. The identified thermal conductivity was compared with existing thermal-conductivity models. Results showed that the combined parallel–series model was more appropriate to describe the combined thermal conductivity due to solid and gas conductions, and the fraction of the fibers oriented parallel to the heat flux for the current sample varied between 0.16 and 0.25 for the investigated temperature range. The identified thermal properties were used to calculate the effective thermal conductivity, which was then compared with the measured result. It was found that most of the predicted effective thermal conductivities using the estimated thermal properties were under-predicted when compared to the measured data. The averaged absolute deviation was around 17.6 %. The identified thermal properties are reliable.

Acknowledgments This work was supported by the National High Technology 863 Projects Foundation of China (No. 2006AA705317). The authors also gratefully acknowledge the financial support of the Center for Composite Materials and Structures of HIT in China.

References

1. C. Stark, J. Fricke, Int. J. Heat Mass Transfer **36**, 617 (1993)
2. D.A. Stewart, D.B. Leiser, P. Kolodziej, M. Smith, J. Spacecr. Rocket **23**, 420 (1986)
3. J.D. Verschoor, P. Greebler, N.J. Manville, J. Heat Transfer **74**, 467 (1952)
4. N.E. Hager, R.C. Steere, J. Appl. Phys. **38**, 4663 (1967)
5. B.K. Larkin, S.W. Churchill, AIChE J. **4**, 467 (1959)
6. T.W. Tong, C.L. Tien, J. Heat Transfer **105**, 70 (1983)
7. T.W. Tong, S.Q. Yang, C.L. Tien, J. Heat Transfer **105**, 70 (1983)
8. J. Marschall, J. Maddren, J. Parks, AIAA 2001-2822
9. K. Daryabeigi, AIAA 1999-1044
10. W.Y. Walter, T. Ezra, C. George, in *The 6th ASME-JSME Thermal Engineering Joint Conference TED-AJ03-126, March 2003*
11. B.M. Zhang, S.Y. Zhao, X.D. He, J. Quant. Spectrosc. Radiat. Transfer **109**, 1309 (2008)
12. V. Giaretto, E. Miraldi, G. Ruscica, High Temp. High Press. **27/28**, 191 (1995/1996)
13. R. Siegel, J.R. Howell, *Thermal Radiation Heat Transfer* (Taylor & Francis, London, 1992)
14. J. Bernard, Am. Math. Mon. **89**, 300 (1982)
15. S.Y. Zhao, B.M. Zhang, S.Y. Du, J. Quant. Spectrosc. Radiat. Transfer **110**, 1111 (2009)
16. E.M. Sparrow, R.D. Cess, *Radiation Heat Transfer,* augmented edn. (McGraw-Hill, New York, 1978), pp. 255–271
17. M.N. Ozisik, *Radiative Transfer and Interactions with Conduction and Convection* (John Wiley&Sons, Inc., New York, 1973)
18. D.W. Marquardt, J. Soc. Ind. Appl. Math. **11**, 431 (1963)
19. K.K. Sun, S.J. Bup, J.K. Hee, L. Woo, Exp. Therm. Fluid Sci. **27**, 697 (2003)
20. I.H. Tavman, Int. Commun. Heat Mass Transfer **25**, 723 (1998)
21. C. Bankvall, J. Test. Eval. **1**, 235 (1973)
22. L.A. Dombrovsky, J. Heat Transfer-T. ASME **118**, 408 (1996)
23. K. Daryabeigi, AIAA Paper, 2001-2834
24. K. Daryabeigi, AIAA Paper, 2002-3332
25. Q.Z. Yu, N. Wen, L.F. Yang, Mater. Sci. Prog. **3**, 249 (1989) [in Chinese]
26. Chinese Metallurgical Standards: Refractory Materials - Determination of Thermal Conductivity (Calorimeter) YB/T 4130-2005 [in Chinese]